Monthly Notices
of the
ROYAL ASTRONOMICAL SOCIETY

Mon. Not. R. Astron. Soc. **416,** 1522–1534 (2011) doi:10.1111/j.1365-2966.2011.19150.x

A possible sequential star formation in the giant molecular cloud G174+2.5

D. Camargo,⋆ C. Bonatto and E. Bica

Departamento de Astronomia, Universidade Federal do Rio Grande do Sul, Av. Bento Gonçalves 9500, Porto Alegre 91501-970, RS, Brazil

Accepted 2011 May 27. Received 2011 May 27; in original form 2010 December 21

ABSTRACT

We investigate the nature of 14 embedded clusters (ECs) related to a group of four H II regions, Sh2-235, Sh2-233, Sh2-232 and Sh2-231, in the giant molecular cloud G174 + 2.5. Projected towards the Galactic anticentre, these objects are possible examples of the *collect-and-collapse* scenario. We derive astrophysical parameters (*age, reddening, distance, core and cluster radii*) for the ECs and investigate the relationship between these parameters. Parameters are derived with field-star-decontaminated 2MASS colour–magnitude diagrams (CMDs) and stellar radial density profiles. The CMDs of these young clusters are characterized by a poorly populated main sequence and a significant number of pre-main-sequence stars, affected by differential reddening. The ECs are KKC 11, FSR 784, Sh2-235 East2, Sh2-235 Cluster, Sh2-233 SE Cluster, BDSB 73, Sh2-235B Cluster, BDSB 72, BDSB 71, Sh2-232 IR Cluster, PCS 2, and the newly found clusters CBB 1 and CBB 2. We were able to derive fundamental parameters for all ECs in the sample. Structural parameters are derived for FSR 784, Sh2-235 Cluster and Sh2-235 East2.

Key words: open clusters and associations: general – Galaxy: stellar content – Galaxy: structure.

1 INTRODUCTION

Most stars form after the gravitational collapse of massive and dense gas clumps inside giant molecular clouds (GMCs), with collapsing clumps forming embedded clusters (ECs). However, supernova explosions, H II region expansion due to massive stars, ultraviolet radiation and stellar winds may disrupt GMCs completely, on a time-scale of a few 10^7 yr (Elmegreen 2000; Bonnell et al. 2006). In this context, Hartmann, Ballesteros-Paredes & Bergin (2001) point out that stars older than ≈5 Myr are not found associated with molecular gas, and Allen et al. (2007) suggest that the primordial gas of ECs disperses in 3–5 Myr (Leisawitz, Bash & Thaddeus 1989; Proszkow & Adams 2009). For Lada & Lada (2003), the duration of the embedded phase is 2–3 Myr. On the other hand, the parent GMCs are very disruptive environments for ECs. Lada & Lada (2003) estimate that only 4–7 per cent of them survive for more than 40 Myr (*infant mortality*), but the appearance of bound and unbound clusters is indistinguishable for clusters younger than 10 Myr. In other words, stars are born in star clusters embedded in GMCs but, as a consequence of the disruptive mechanisms, most end up as part of the field-star population after cluster disruption.

ECs can be partially or fully immersed in embryonic molecular clouds and H II regions. The youngsters are located in gas clumps and the most evolved are often linked with H II regions or other nebulae (Leisawitz et al. 1989). Often, these H II regions, excited by fast winds from massive OB stars, expand into the molecular cloud triggering sequential star formation. In this sense, the *collect-and-collapse* model (Elmegreen & Lada 1977; Whitworth et al. 1994) suggests that H II regions expand accumulating material between the ionization and the shock fronts. This material, as a consequence of the shocks, becomes unstable and fragments into several cores, triggering star formation in multiple protocluster regions. Another possible process is the 'radiation-driven implosion' model, in which the expanding H II region compresses the existing molecular clumps, the density increases, exceeding the critical mass, and the clump collapses (Lefloch & Lazareff 1994). In both scenarios, the massive stars trigger a second generation of cluster formation (see also, Fukuda & Hanawa 2000; Deharveng, Zavagno & Caplan 2005; Hosokawa & Inutsuka 2005; Dale, Bonnell & Whitworth 2007). In any case, GMC observations indicate that there often occurs a multiple-cluster formation as a result of winds of OB stars or expanding H II regions (Allen et al. 2007).

Star cluster formation is the preferential mode of star formation, and ECs may be responsible for 70–90 per cent of all stars formed in GMCs. However, the rapid expulsion of the primordial gas by winds of OB stars and supernova explosions disrupt most clusters very early. As a consequence of rapid gas expulsion, the stellar orbits cannot adjust to the new potential and probably give rise to an unbound association. *N*-body simulations show that in this

⋆E-mail: denilso.camargo@ufrgs.br

phase (10–30 Myr) the cluster expands in all scales reaching for virialization. The fate of a cluster is determined by the star formation efficiency (SFE). If the gas is removed slowly, the cluster will remain bound as long as the SFE is higher than 30 per cent, but if the gas is removed rapidly, the SFE needs to be higher than 50 per cent. As a consequence of *infant mortality*, the number of optically detected clusters is significantly smaller than that of ECs (Lada, Margulis & Dearborn 1984; Verschueren 1990; Lada & Lada 2003; Goodwin & Bastian 2006).

Young clusters in expanding H II regions are characterized by a significant population of low-mass pre-main-sequence (PMS) stars together with variable fractions of massive OB stars (Saurin, Bica & Bonatto 2010; Bonatto & Bica 2011). Dobashi et al. (2001) show that protostars associated with H II regions are more luminous than those in molecular clouds away from them, which indicates that H II regions favour massive stars or cluster formation in neighbouring molecular clouds. Deharveng et al. (2003) suggest that clusters formed from these processes are still deeply embedded in H II regions and are not dispersed.

The observed colour–magnitude diagram (CMD) of an EC in general presents a relatively vertical, poorly populated main-sequence (MS) and a well-developed PMS with a large population of faint and red stars (Bonatto & Bica 2009). This feature is evident when the raw photometry and decontaminated CMDs are compared to field-star extractions in the present analysis. The low-mass stars remain in the PMS phase for ≈30 Myr (Gouliermis et al. 2008).

In this work, we investigate properties of the star clusters embedded in the GMC G174 + 2.5, related to a group of H II regions located in the Perseus arm towards the Galactic anticentre. A star-forming complex with numerous ECs minimizes uncertainties owing to the distance in common. This paper is organized as follows. In Section 2, we provide general data on the target clusters. In Section 3, we present the 2MASS photometry and introduce tools employed in the CMD analyses, especially the field-star-decontamination algorithm. Section 4 is dedicated to the cluster structure. In Section 5, we estimate cluster masses. In Section 6, we investigate the relationship between the derived parameters. Finally, in Section 7, we present the concluding remarks.

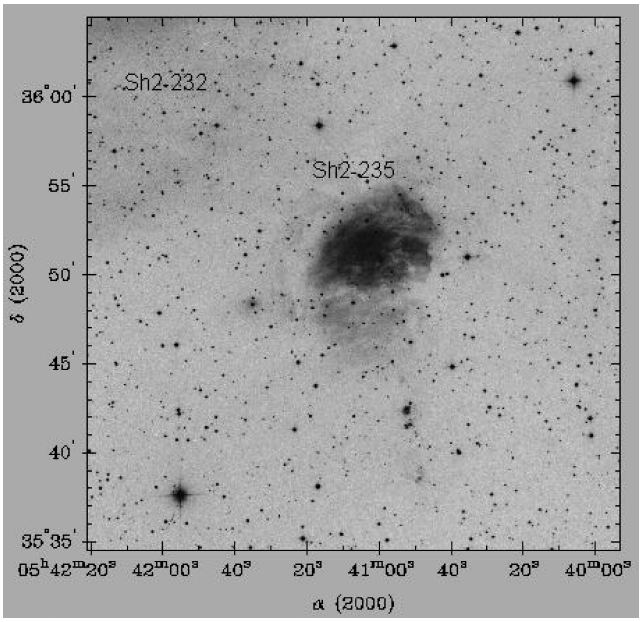

Figure 1. XDSS *R* image (30 × 30 arcmin^2) of the Sh2-235 H II region. The image also shows part of the Sh2-232 H II region (top left-hand side).

2 PREVIOUS STUDIES ON THE G174+2.5 STELLAR CONTENT

The H II regions Sh2-235, Sh2-233, Sh2-232 and Sh2-231 have been subject to several studies in different wavelength ranges, but astrophysical parameters for most ECs located in these regions have not been derived so far. The ECs selected for the present analysis are given in Table 1, where we adopt a chronological criterion for the literature identifications. We show in Fig. 1 an XDSS 30 × 30 arcmin^2 *R* image of the Sh2-235 H II region. In Fig. 2, we show schematic charts for the nebulosities and clusters, and in Fig. 3, 2MASS images of the ECs in the K_S band. All objects are quite obscured by interstellar dust and appear to be affected by differential reddening.

Table 1. Cross-identifications of the ECs in G174 + 2.5.

Desig#1 (1)	Desig#2 (2)	Desig#3 (3)	Desig#4 (4)	Desig#5 (5)	*D* (arcmin) (6)	Reference (7)
KKC 11	FSR 788	Sh2-235 East1	–	–	4.5	7, 8, 10
FSR 784	Koposov 7	Sh2-235 North-West	–	–	3.2	8, 9, 10
Sh2-235 East2	–	–	–	–	1.3	6
Sh2-235 Cluster	CSSS 11	Sh2-235 Central	–	–	1.4	1, 10
BDSB 73	KSTW 1	–	–	–	0.7	5, 8
Sh2-235B Cluster	CSSS 10	Hodapp 18	Sh2-235ABC Cluster	–	1.6	1, 2, 10
BDSB 72	–	–	–	–	2.0	6
BDSB 71	–	–	–	–	0.8	6
Sh2-232 IR Cluster	–	–	–	–	1.0	10
PCS 2	DB2001-24	KKC 9 NE	–	–	1.0	3, 4, 7
Sh2-233 SE Cluster	Hodapp 15	PCS 1	KKC 9 SW	Sh2-233 IR Cluster	1.1	2, 3, 6, 10
G173.58 + 2, 45 Cluster	IRAS 05361 + 3539 Cluster	–	–	–	0.5	5, 10
CBB 1	–	–	–	–	0.3	11
CBB 2	–	–	–	–	1.0	11

Notes. Columns (1)–(5) show cross-identification and column (7) shows references for parameter determinations. The references are: 1 – Carpenter et al. (1993); 2 – Hodapp (1994); 3 – Porras, Cruz-Gonzàles & Salas (2000); 4 – Dutra & Bica (2001); 5 – Shepherd & Watson (2002); 6 – Bica et al. (2003); 7 – Kumar, Keto & Clerkin (2006); 8 – Froebrich, Scholz & Raftery (2007); 9 – Koposov, Glushkova & Zolotukhin (2008); 10 – Kirsanova et al. (2008); 11 – This work.

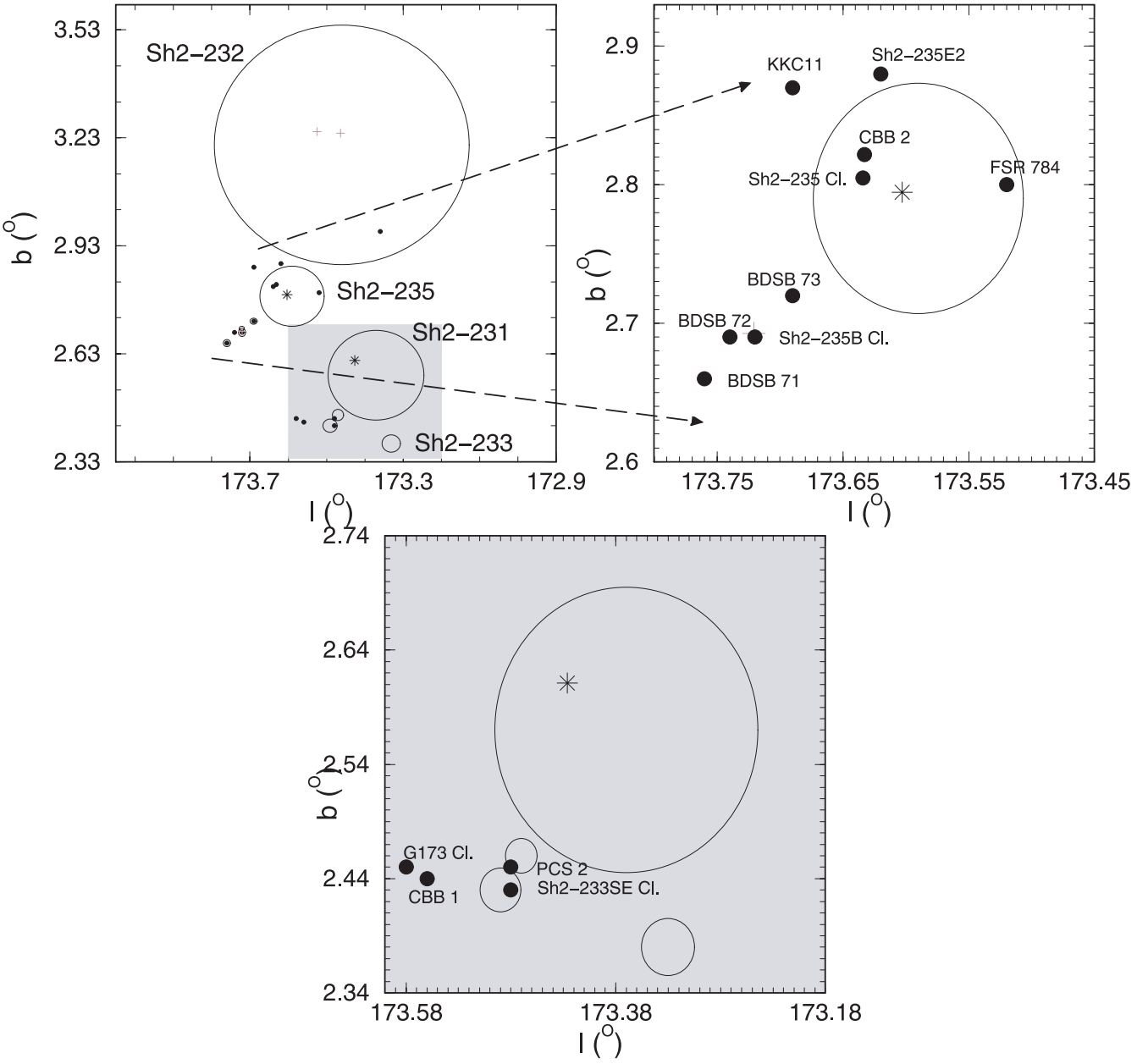

Figure 2. Top left-hand panel: schematic map of the nebulae (open circles). The filled circles are ECs, asterisks are O stars and plus signs are B stars. Top right-hand panel: zoom-in of the region that contains the H II region Sh2-235 Cluster. Bottom panel: zoom-in of the grey region in the top left-hand panel that contains the nebulae Sh2-231, Sh2-233, RNO49 and Sh2-233 SE Cluster.

Being projected close to each other, this sample of ECs may be an example of H II regions with a sequential star formation and the development of a *collect-and-collapse* scenario. Furthermore, the detection of far-IR sources, molecular outflows and H_2O masers in previous works indicates ongoing star formation. The distance from the Sun estimated for these H II regions is in the range $d_\odot$ = 1.0–2.3 kpc (Georgelin 1975). Most works use $d_\odot = 1.8$ kpc for this group of nebulosities.

Within uncertainties, Sh2-231, Sh2-232, Sh2-233 and Sh2-235 have comparable CO radial velocities (Blitz, Fich & Stark 1982). This indicates that we are dealing with a large H II molecular complex with components located essentially at the same distance from the Sun.

2.1 Sh2-235 and surroundings

Sh2-235 is the most prominent H II region in this group. It is a diffuse optical H II region excited by a star of spectral type O9.5 V (BD +35°1201). Allen et al. (2005) identify two clusters associated with the Sh2-235 H II region, Sh2-235 Cluster and KKC 11. Kumar et al. (2006) add to these objects the cluster Sh2-235 East2. Kirsanova et al. (2008) conclude that these objects are still embedded in dense clumps of the parental molecular cloud G174 + 2.5. They also argue that Sh2-235 Cluster and Sh2-235 East2 probably started primordial gas expulsion, but KKC 11 is less evolved.

South-west of Sh2-235 Cluster are four small nebulae named GGD 6 (also known as RNO 52), Sh2-235A Cluster (GM1-G6),

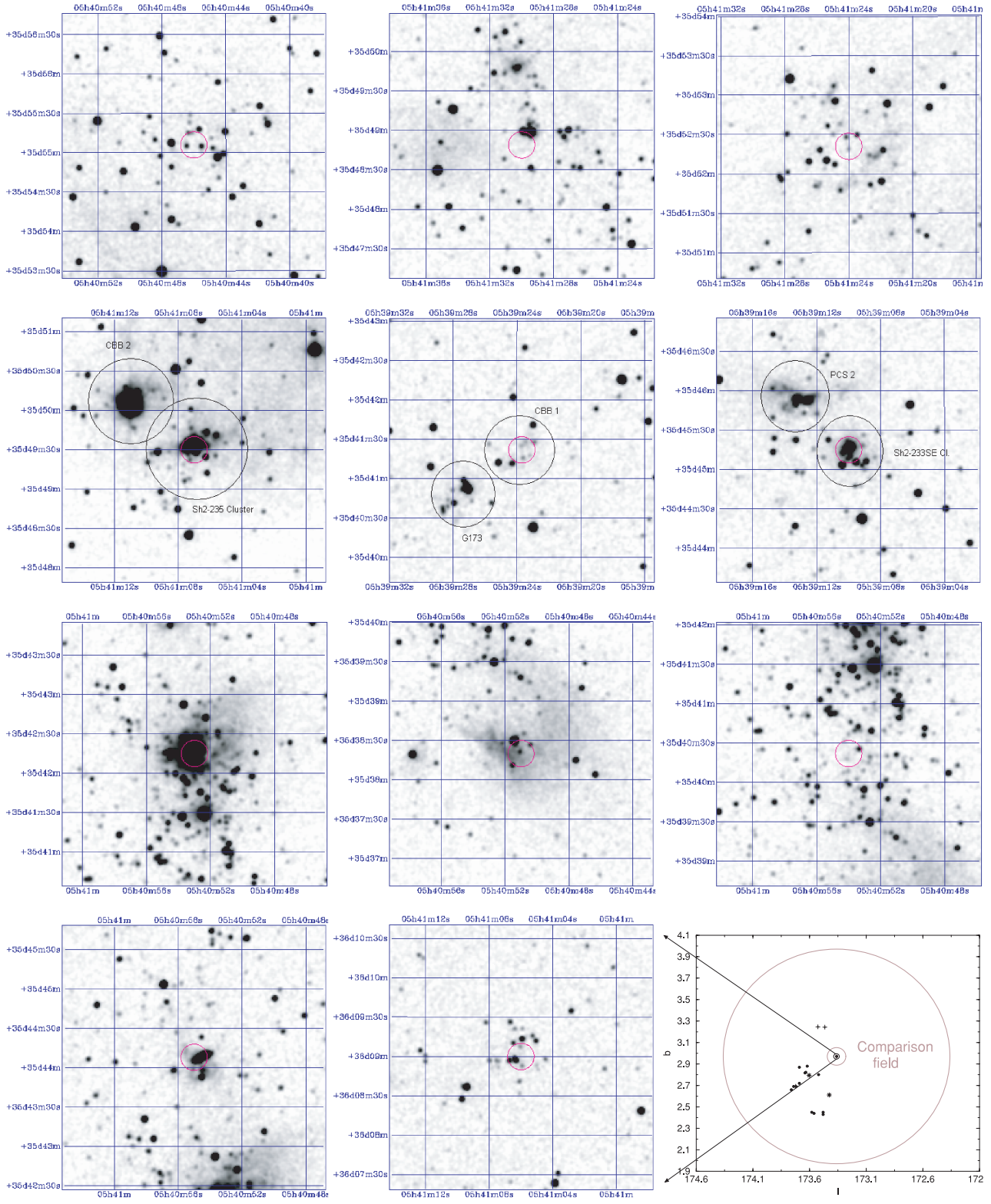

Figure 3. First row panels: 2MASS 3 × 3 arcmin^2 K_S images centred on FSR 784, KKC 11 and Sh2-235 East2. Second row panels: the same for the cluster pairs Sh2-235 Cluster and CBB 2, G173 and CBB 1, and PCS 2 and Sh2-233 SE Cluster. Third row of panels: Sh2-235B Cluster, BDSB 71 and BDSB 72. Fourth row of panels: same as the third row, but for BDSB 73 and Sh2-232 IR Cluster. The small circle is automatically generated by the 2MASS image tool, surrounding the input coordinates. The large circle in the second row surrounds the main body of each cluster. The rightmost panel in the fourth row shows the large background area (indicated with the outer and inner brown circles) used in the statistical field decontamination of Sh2-232 IR Cluster. Note that it is huge with respect to the cluster area, for statistical purposes. The symbols are the same as in Fig. 2.

Table 2. Derived fundamental parameters for the ECs.

Cluster	α(2000) (h m s)	δ(2000) (° ′ ″)	ℓ (°)	b (°)	A_V (mag)	Age Myr	$d_\odot$ (kpc)	R_{GC} (kpc)
(1)	(2)	(3)	(4)	(5)	(6)	(7)	(8)	(9)
KKC 11	5:41:30	35:48:49	173.685	2.865	5.5 ± 1.0	3 ± 2	2.2 ± 0.5	9.4 ± 0.2
FSR 784	5:40:46	35:55:06	173.517	2.794	4.0 ± 1.0	3 ± 2	2.4 ± 0.5	9.6 ± 0.2
Sh2-235 East2	5:41:24	35:52:21	173.624	2.878	4.0 ± 1.0	3 ± 2	2.1 ± 0.5	9.3 ± 0.2
Sh2-235 Cluster	5:41:07	35:49:30	173.634	2.805	3.8 ± 1.0	5 ± 2	2.0 ± 0.6	9.2 ± 0.2
BDSB 73	5:40:55	35:44:08	173.688	2.723	3.8 ± 1.0	3 ± 2	2.1 ± 0.5	9.3 ± 0.5
Sh2-235B Cluster	5:40:53	35:42:15	173.712	2.701	3.8 ± 1.0	3 ± 2	1.9 ± 0.5	9.1 ± 0.5
BDSB 72	5:40:54	35:40:22	173.740	2.687	3.8 ± 1.0	3 ± 2	2.1 ± 0.5	9.3 ± 0.5
BDSB 71	5:40:51	35:38:20	173.763	2.660	3.8 ± 1.0	3 ± 2	2.0 ± 0.4	9.2 ± 0.4
Sh2-232 IR Cluster	5:41:06	36:09:00	173.356	2.973	5.0 ± 1.2	3 ± 2	1.9 ± 0.5	9.1 ± 0.5
PCS 2	5:39:13	35:45:53	173.481	2.446	3.5 ± 1.0	3 ± 2	2.2 ± 0.5	9.4 ± 0.5
Sh2-233 SE Cluster	5:39:10	35:45:15	173.484	2.432	3.5 ± 0.8	3 ± 2	2.2 ± 0.5	9.4 ± 0.5
G173	5:39:28	35:40:43	173.581	2.443	3.5 ± 0.9	5 ± 3	2.5 ± 0.2	9.8 ± 0.2
CBB 1	5:39:23	35:41:22	173.563	2.434	3.5 ± 0.9	5 ± 3	2.5 ± 0.2	9.8 ± 0.2
CBB 2	5:41:11	35:50:10	173.632	2.822	3.8 ± 1.0	3 ± 2	2.0 ± 0.6	9.2 ± 0.2

Notes. Columns (2)–(5): optimized central coordinates; Column (6): reddening in the cluster's central region; Column (7): age, from 2MASS photometry; Column (8): distance from the Sun; and Column (9): R_{GC} calculated with $R_\odot = 7.2$ kpc (Bica et al. 2006) as the distance of the Sun from the Galactic Centre. The ECs CBB 1 and CBB 2 were discovered in this work.

Sh2-235B Cluster (BFS 46 or GM1-G5) and Sh2-235C Cluster (GGD 5 or BFS 47). Sh2-235A Cluster and Sh2-235B Cluster are located at about 10 arcmin (5.6 pc) south of Sh2-235 Cluster and separated by ≈40 arcsec (0.35 pc) (Blitz et al. 1982). Sh2-235A Cluster is a compact H II region of ≈20 arcsec (0.17 pc) in diameter (Felli et al. 1997). For Boley et al. (2009), the exciting star of Sh2-235B Cluster is an early-type Herbig Be star of spectral type B1V. Hodapp (1994) found a cluster in Sh2-235B Cluster, which was confirmed by Wang, Testi & Felli (1997), Allen et al. (2005) and Kirsanova et al. (2008). Sh2-235C Cluster is a small H II region located at about 3.5 arcmin south of Sh2-235B Cluster (Felli et al. 2004). It coincides with an optical nebula and is excited by a B0.5 star, presenting a Herbig–Haro object and a partial shell morphology (Felli et al. 1997). Bica et al. (2003) identify other three ECs in these nebulosities, BDSB 71, 72 and 73.

Based on the spatial distribution of clusters and kinematics of molecular gas, Kirsanova et al. (2008) point out that the expansion of Sh2-235 Cluster would be responsible for cluster formation in that area. They suggest that sequential star formation is triggered by a combination of the compression of pre-existing dense clumps by the shock wave and the *collect-and-collapse* scenario. However, the clusters in Sh2-235A Cluster, Sh2-235B Cluster and Sh2-235C Cluster appear to be embedded in primordial gas, and star formation cannot be triggered by the expansion of the Sh2-235 Cluster ionization front (Lafon et al. 1983). On the other hand, Tokunaga & Thompson (1979) suggest that the linear disposition of these star-forming regions may be the result of the *collect-and-collapse* scenario.

2.2 Sh2-231, Sh2-232 and Sh2-233

Sh2-232 is an extended H II region with ≈40 arcmin diameter (Fig. 2), excited by B stars. Hodapp (1994) observed two nebulae in Sh2-233 and noted a young infrared EC, as well as a probable Herbig–Haro object. Porras et al. (2000) identified two clusters in this region, PCS 2, located around the IRAS 05358 + 3543 source, and Sh2-233 SE Cluster at a separation of 1 arcmin (0.5 pc) from each other for an adopted distance from the Sun of 1.8 kpc. However, Chan & Fich (1995) estimated a distance of 2.3 ± 0.7 kpc, based on spectral types of stars in the H II region. Porras et al. (2000) detected 92 stars in JHK_S, but those associated to PCS 2 and Sh2-233 SE Cluster are 20 and 15 in number, respectively. The average extinction was $A_V = 8.44 \pm 4.77$ for Sh2-233 SE Cluster and $A_V = 15.06 \pm 3.48$ for PCS 2. The estimated ages were 6 Myr for field stars, 3 Myr for Sh2-233 SE Cluster and less than 2 Myr for PCS 2. Mao & Zeng (2004), based on cluster members (Porras et al. 2000), obtained a stellar mass of 10.7 $M_\odot$ for PCS 2 with a SFE of ∼4 per cent, and for Sh2-233 SE Cluster a mass of 38.4 $M_\odot$ with a SFE of ∼47 per cent. They suggest that the SFE of PCS 2 was underestimated because of the upper mass completeness limit of 1 $M_\odot$ estimated for PCS 2 and point out that the SFE increases with time while the cluster is embedded in a molecular cloud. The large SFE difference between the two clusters indicates that Sh2-233 SE Cluster is more evolved than PCS 2. Snell, Dickman & Huang (1990) identified a CO outflow with two lobes centred on IRAS 05358 + 3543. Jiang et al. (2001) named Sh2-233 SE Cluster and PCS 2 as S233 A and S233 B, respectively. They argue that Sh2-233 SE Cluster is less embedded than PCS 2. Recently, Yan et al. (2010) derived ages of 0.3, 0.5 and 1.5 Myr and masses of 45, 30 and 107 $M_\odot$ for Sh2-233 SE Cluster, PCS 2 and field stars, respectively.

The nebula G173.58 + 2.45 shows multiple outflow sources, typical of regions presenting young stellar objects (YSOs) (Wouterloot & Brand 1989; Shepherd & Churchwell 1996; Shepherd & Watson 2002; Varricatt, Davis & Adamson 2005). The most extended jet appears to be associated with a binary system near the centre of the G173.58+2.45 cluster (hereinafter G173). We discovered an additional EC, CBB 1, at an angular distance of 1 arcmin from G173.

3 2MASS PHOTOMETRY

2MASS[1] photometry (Skrutskie et al. 2006) in the J, H and K_S bands was extracted in concentric regions centred on the coordinates of the ECs (Table 2) using VizieR.[2] Large extraction areas are essential to

[1] The Two-Micron All-Sky Survey, available at www.ipac.caltech.edu/2mass/releases/allsky/

[2] http://vizier.u-strasbg.fr/viz-bin/VizieR?-source=II/246.

build radial density profile (RDPs) (Section 4) with a high resulting contrast relative to the background and for a consistent field-star decontamination (Section 3.1).

3.1 Field-star decontamination

Field stars are conspicuous in the observed CMDs of the present ECs (Figs 4–8). To uncover the intrinsic CMD morphology from the field stars, we apply a field-star-decontamination procedure. The algorithm deals statistically with the relative number densities of probable cluster and field stars in cubic CMD cells that have axes along the J, $(J - H)$ and $(J - K_S)$ axes. These are the colours that provide the maximum discrimination among CMD sequences for star clusters of different ages (e.g. Bonatto, Bica & Girardi 2004).

The algorithm (i) divides the range of magnitude and colours of a given CMD into a 3D grid, (ii) computes the expected number density of field stars in each cell based on the number of comparison field stars (within 1σ Poisson fluctuation) with magnitude and colours compatible with those of the cell, and (iii) subtracts from each cell a number of stars that correspond to the number density of field stars measured within the same cell in the comparison field. Consequently, this method is sensitive to local variations in field-star contamination in magnitude and colours. Cell dimensions are $\Delta J = 1.0$ and $\Delta(J - H) = \Delta(J - K_S) = 0.2$, which provide sufficient star-count statistics in individual cells and preserve the morphology of the CMD evolutionary sequences. The dimensions of the colour/magnitude cells can be subsequently changed so that the total number of stars subtracted in the whole cluster area matches the expected one (1σ Poisson fluctuation). We give a brief description of the field-star-decontamination procedure. For details, see Bonatto & Bica (2007a) and Bica, Bonatto & Camargo (2008).

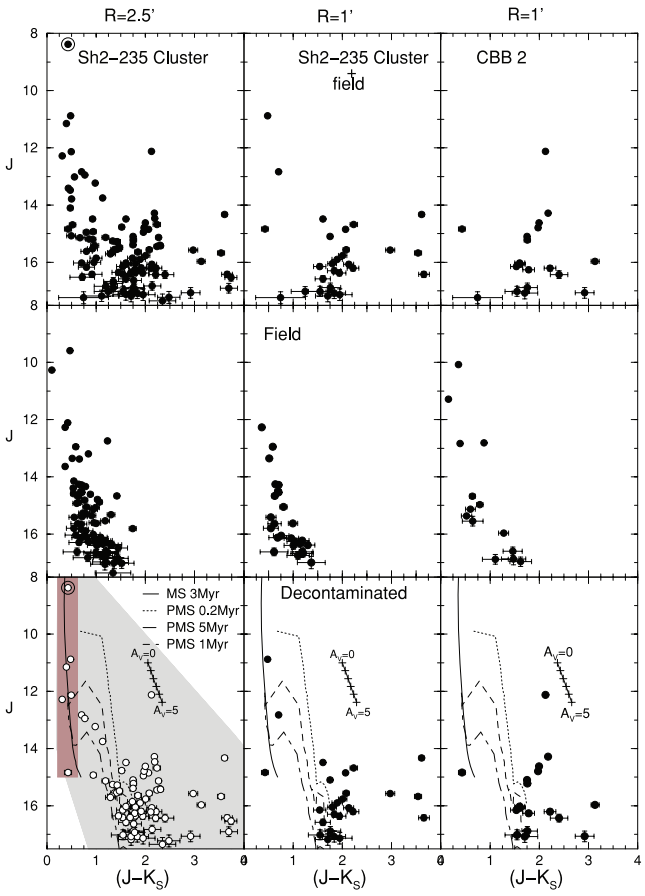

Figure 4. 2MASS CMDs extracted from the central regions of the cluster pair Sh2-235 Cluster and CBB 2. Top panels: observed CMDs $J \times (J - K_S)$. Middle panels: equal-area comparison field. Bottom panels: field-star-decontaminated CMDs fitted with the Padova isochrone for MS stars and the Siess, Dufour & Forestini (2000) isochrone for PMS stars. The CM filters used to isolate cluster MS and PMS stars are shown as the shaded regions. We also present the reddening vector for $A_V = 0$–5. BD +35°1201 is shown as a circle around the star in the top and bottom left-hand panels.

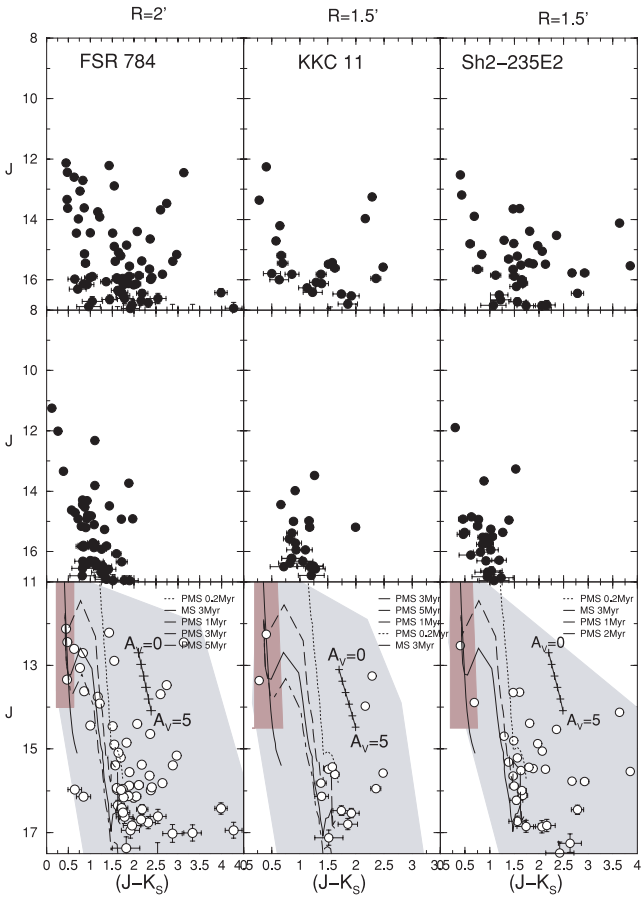

Figure 5. 2MASS CMDs extracted from the central regions of FSR 784, KKC 11 and Sh2-235 East2, respectively. Top panels: observed CMDs $J \times (J - K_S)$. Middle panels: equal-area comparison field. Bottom panels: field-star-decontaminated CMDs fitted with the Padova isochrone for MS stars and the Siess, Dufour & Forestini (2000) isochrone for PMS stars. The CM filters used to isolate cluster MS and PMS stars are shown as the shaded regions. We also present the reddening vector for $A_V = 0$–5.

3.2 Fundamental parameters

Usually, decontaminated CMDs of ECs are characterized by a poorly populated MS and a significant number of PMS stars. PMS stars are usually located in the same CMD region occupied by faint red field stars and consequently one is not able to distinguish them, considering only CMD properties. In this context, the field-star-decontamination procedure is essential for the identification of cluster evolution sequences. We adopt isochrones from the Padova group with solar metallicity (Girardi et al. 2002) computed with the 2MASS J, H and K_S filters, and the PMS tracks of Siess et al. (2000) fitted in $J \times (J - H)$ and $J \times (J - K_S)$ decontaminated CMDs (Figs 4–8) to derive the ECs' fundamental parameters. Because of

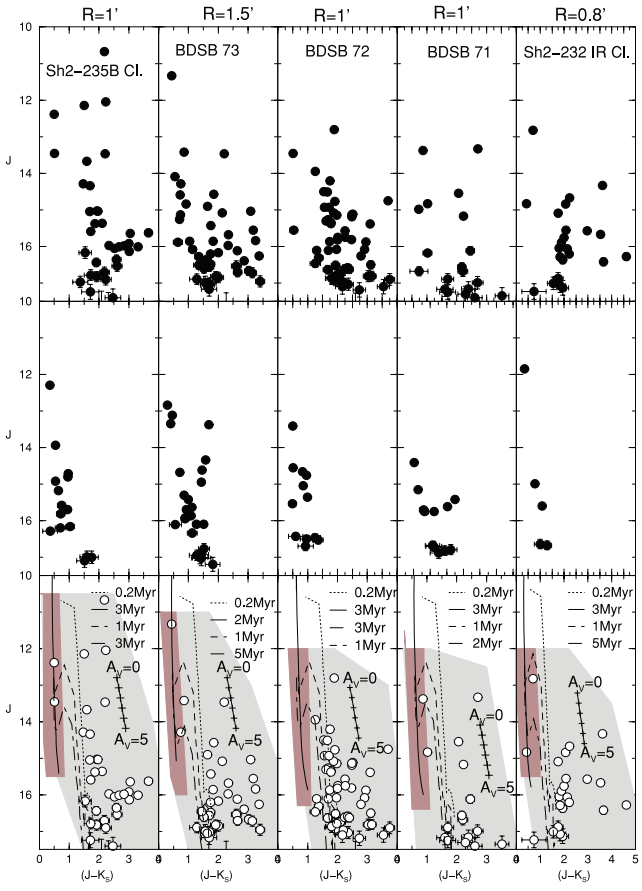

Figure 6. Same as Fig. 5, but for Sh2-235B Cluster, BDSB 73, BDSB 72, BDSB 71 and Sh2-232 IR Cluster, respectively.

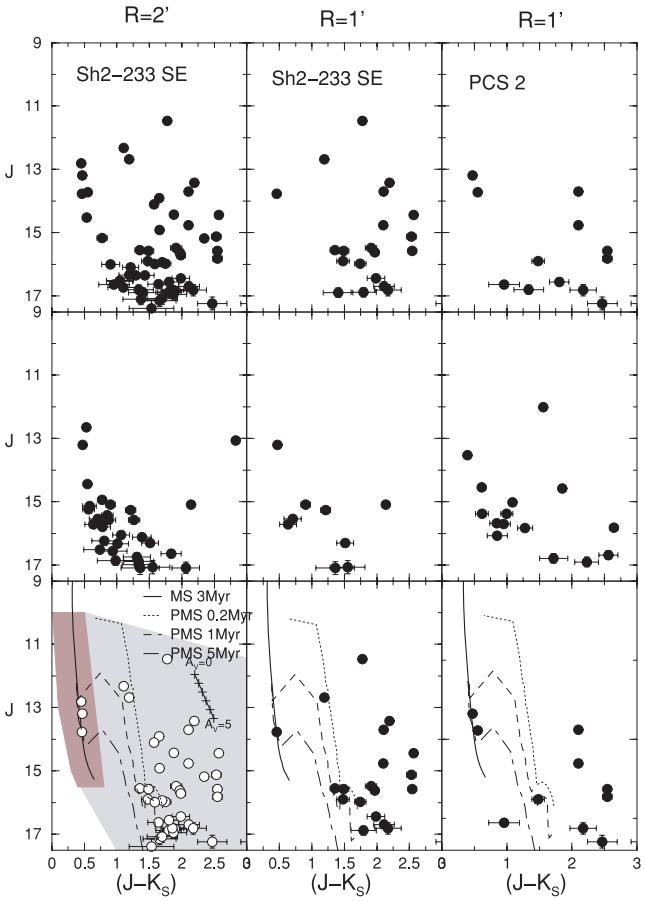

Figure 7. Same as Fig. 4, but for the cluster pair PCS 2 and Sh2-233 SE Cluster.

the poorly populated MSs, the 2MASS photometric uncertainties for lower sequences, the large population of PMS stars and differential reddening, we decided for the direct comparison of isochrones with the decontaminated CMD morphology. We carry out eye fits, taking the combined MS and PMS stellar distribution as a constraint, allowing for differential reddening and photometric uncertainties. The cluster sample presents a significant fraction of stars redder than the youngest PMS isochrone. Probably, the differential reddening contributed to this $(J - K_S)$ excess towards red colours, but part of it can be intrinsic and related to their evolutionary stage. The youngest stars are the reddest and with evolution their colours become bluer and move towards the MS (Lada & Adams 1992). Most of these redder stars have infrared excesses owing to discs. The isochrone fit gives the observed distance modulus $(m - M)_J$ and reddening $E(J - H)$, which converts to $E(B - V)$ and A_V with the relations $A_J/A_V = 0.276$, $A_H/A_V = 0.176$, $A_{K_S}/A_V = 0.118$, $A_J = 2.76 \times E(J - H)$ and $E(J - H) = 0.33 \times E(B - V)$ (Dutra, Santiago & Bica 2002). We estimate A_V assuming a constant total-to-selective absorption ratio $R_V = 3.1$ and adopt the Sun's distance from the Galactic Centre $R_\odot = 7.2$ kpc (Bica et al. 2006). The resulting A_V, age, $d_\odot$ and R_{GC} values are given in columns 4, 5, 6 and 7 of Table 2, respectively. We also present in the field subtracted CMDs the reddening vector for $A_V = 0$–5.

In Fig. 4, we show the CMDs of the cluster pair Sh2-235 Cluster ($R = 2.5$ and 1 arcmin) and CBB 2 ($R = 1$ arcmin). The aim of this procedure is to isolate the population of each EC and discard the possibility that we may be working with a single object. In the top panels, we present the $J \times (J - K_S)$ CMDs extracted for Sh2-235 Cluster and CBB 2. In the middle panels, we show the background field corresponding to a ring with the same area as the central region. In the bottom panels, we give the field-star-decontaminated CMDs. For the ensemble, we get $A_V = 3.77 \pm 1.0$ mag and a distance from the Sun $d_\odot = 2.0 \pm 0.1$ kpc, which agrees with previous values (Georgelin, Georgelin & Roux 1973).

Fig. 5 presents the $J \times (J - K_S)$ CMDs for FSR 784, KKC 11 and Sh2-235 East2. These objects are very young clusters characterized by the presence of a poorly populated MS and a larger number of PMSs that appear to be very reddened. These features are absent in the comparison field. The gap between the MS and PMS is characteristic of young clusters. The combination of the MS and PMS shows that these objects are ECs.

We show in Fig. 6 the CMDs of the ECs Sh2-235B Cluster, BDSB 73, BDSB 72, BDSB 71 and Sh2-232 IR Cluster. These objects present a poorly populated MS and a rather populous PMS.

Figs 7 and 8 show the CMDs of cluster pairs. Fig. 7 shows the CMDs of the pair PCS 2 ($R = 1$ arcmin) and Sh2-233 SE Cluster ($R = 2$ and 1 arcmin). Fig. 8 presents the CMDs of the pair CBB 1 ($R = 1$ arcmin) and G173 ($R = 2$ and 1 arcmin). Both objects present CMDs characteristic of very young clusters. The pair separations are small and have a number of stars in common (see Fig. 9). We do not discard the possibility that these two objects will merge. $d_\odot = 2.2 \pm 0.5$ kpc for Sh2-233 SE Cluster agrees with $d_\odot = 2.3 \pm 0.7$ estimated by Chan & Fich (1995). The diamond in the CMD of G173 is the IRAS 05361+3539 source (Section 2), which appears to be a PMS star approaching the MS.

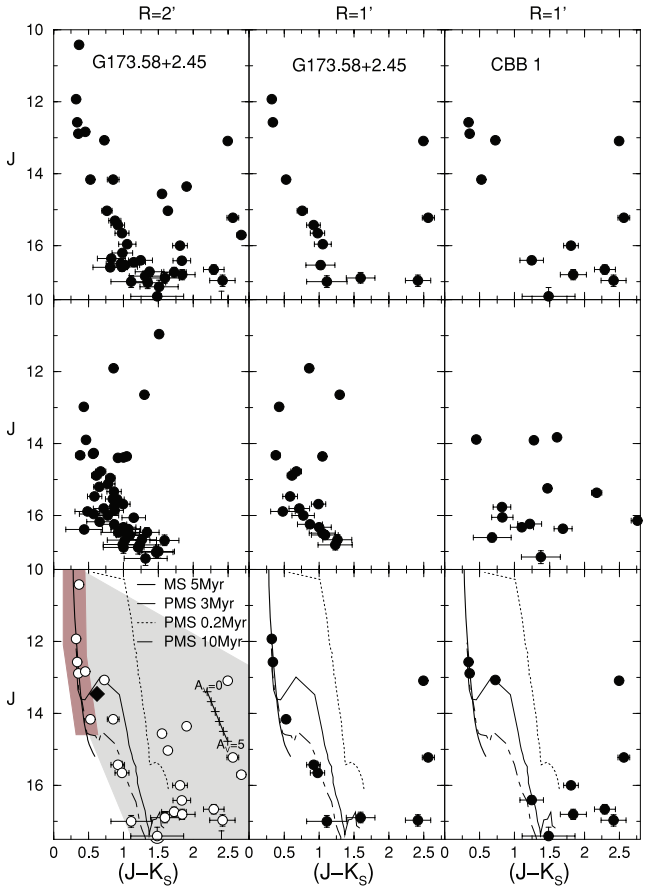

Figure 8. Same as Fig. 4, but for the cluster pair G173 and CBB 1. The diamond is the IRAS 05361+3539 source.

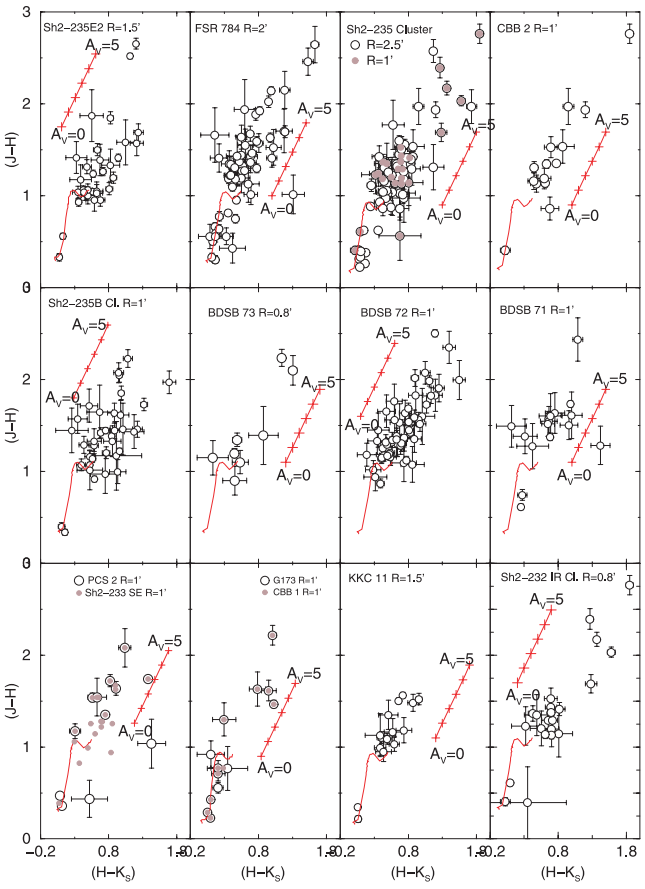

Figure 9. Colour–colour diagrams for the decontaminated photometry. Siess et al. (2000) isochrones and reddening vectors are compared with the PMS distribution.

We estimate A_V for BDSB 71 and Sh2-233 SE Cluster assuming a constant total-to-selective absorption ratio $R_V = 5.0$, which is typical of dense clouds (Cardelli, Clayton & Mathis 1989). BDSB 71 presents $A_V = 6.0 \pm 1.6$ mag for a distance from the Sun of $d_\odot = 1.3 \pm 0.7$ kpc. For Sh2-233 SE Cluster, the values are $A_V = 6.4 \pm 1.6$ mag and $d_\odot = 1.6 \pm 0.5$ kpc.

Fig. 10 shows the number density distribution for probable stars in the decontaminated $J \times (J - K_S)$ CMDs. The densest parts of those Hess diagrams correspond to the PMS.

The present sample of ECs suggest some age spread implied mainly by the PMS stars. This suggests some sequential star formation (Fig. 11). However, the visual extinction of the same ECs is much smaller than the values observed for individual stars in these clusters which suggests that these stars are probably embedded in dense structures, which explains the larger values of A_V estimated in the previous works, especially in the case of individual star analyses.

Figs 2, 3 and 11, together with the age derived for Sh2-235 Cluster (≈5 Myr), indicate that the O star (≈1 Myr) is not a member of this cluster. A possible explanation for the presence of the O star near this cluster is that winds from Sh2-235 Cluster, colliding with the surrounding gas, might have originated this star, CBB 2 and other clusters in the neighbourhood. Assuming $v \approx 20\,\mathrm{km\,s^{-1}}$ for the dense gas involved in the expansion (Kirsanova et al. 2008), Sh2-235 Cluster might be responsible for sequential star formation across a region of radius ≈ 10 pc (Fig. 11), which includes also the clusters in a row in the south-west direction. Sequential star formation is possible also for the pairs G173 and CBB 1, and Sh2-233 SE Cluster and PCS 2. Recently, Dewangan & Anandarao (2011) point out that star formation continues to occur in the Sh2-235 complex, mainly within the ECs. They identified 86 Class 0/I and 144 Class II YSOs, which reinforce the possibility of a sequential star formation event.

3.3 Colour–colour diagrams

Colour–colour diagrams are useful tools to investigate the nature of ECs. We show in Fig. 9 the decontaminated near-IR colour–colour diagram $(J - K_S) \times (H - K_S)$ of the member stars, together with PMS tracks (Siess et al. 2000), set with the reddening values derived above, to estimate ages. As a consequence of the presence of the PMS stars in the cluster, it is expected that some stars present near-IR excess. As expected from the CMDs of ECs (Figs 4–8), a significant fraction of the stars appear to be very reddened. Most stars, specially MS stars, have $(H - K_S)$ colours close to the isochrone, within the uncertainties. Besides, most of the very red PMS stars are displaced parallel to the respective reddening vectors. However, a significant fraction appear to present an abnormal excess in $(J - K_S)$ and $(H - K_S)$, especially Sh2-235B Cluster, which may come from PMS stars still bearing circumstellar discs. MS stars lie on the blue side of the diagrams and there occurs a gap between MS and PMS stars in the CMDs.

4 CLUSTER STRUCTURE

The structure of the ECs is analysed by means of the stellar RDP, defined as the projected number of stars per area surrounding the

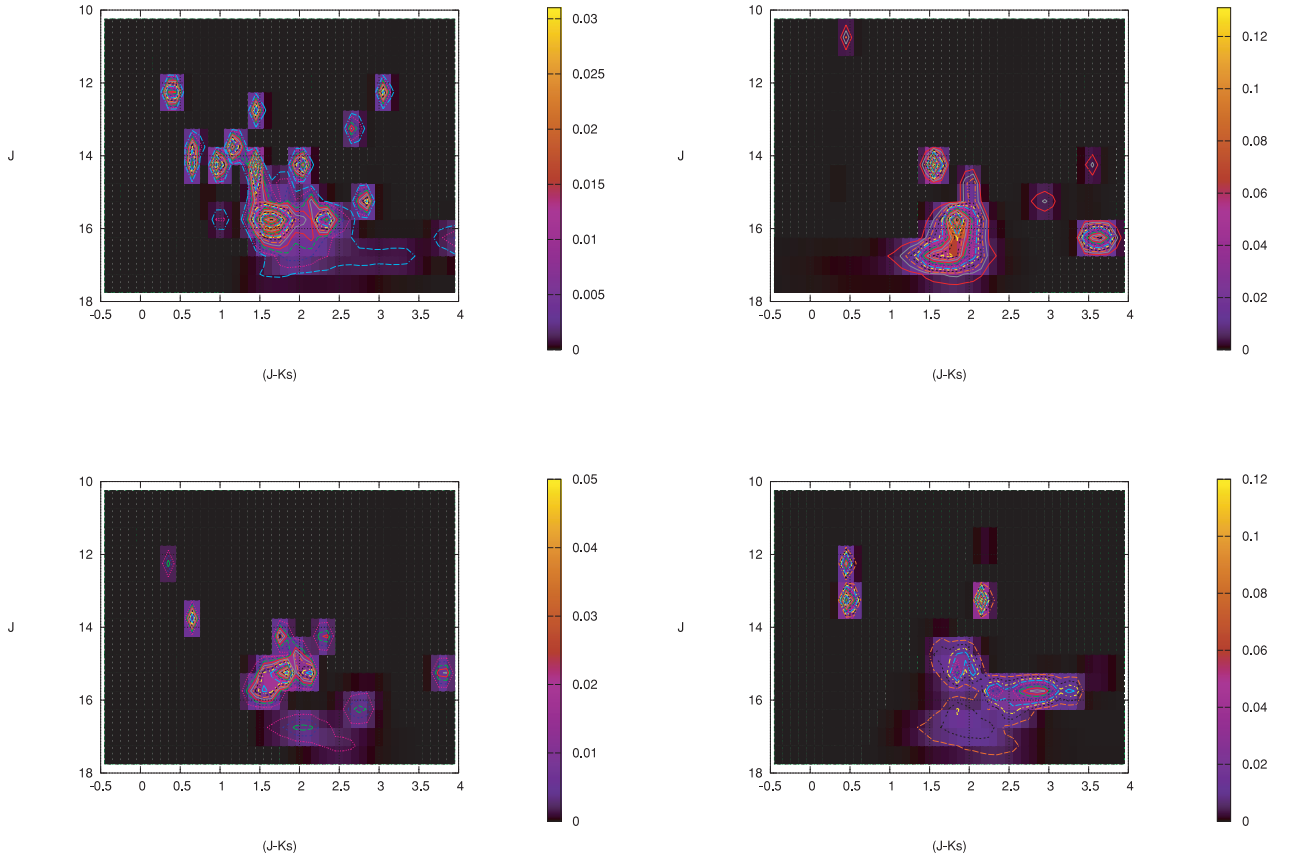

Figure 10. Number density (stars arcmin^{-2}) distribution for probable stars present in the decontaminated CMDs of FSR 784 (top left-hand panel), Sh2-235 Cluster (top right-hand panel), Sh2-235 East2 (bottom left-hand panel) and Sh2-235B Cluster (bottom right-hand panel).

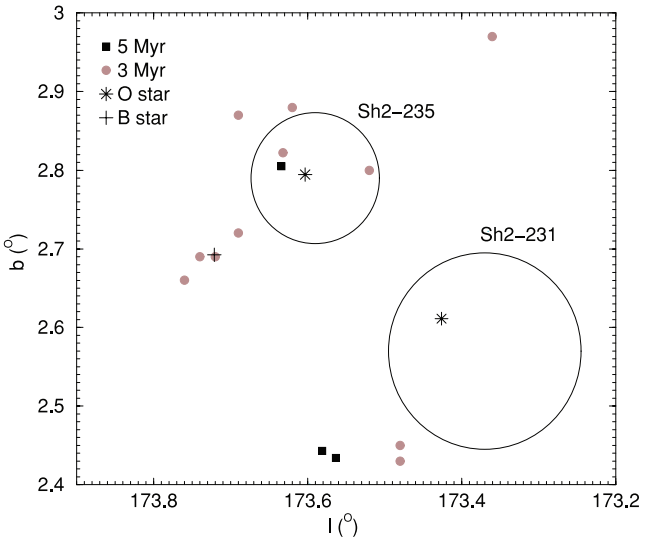

Figure 11. Schematic distribution of cluster positions and ages. The asterisks are O stars and the plus sign is a B star. It also shows the nebulae Sh2-235 Cluster and Sh2-231 for reference.

cluster centre. RDPs are built with stars selected after applying the respective colour–magnitude (CM) filter to the observed photometry. CM filters isolate the probable cluster sequences, excluding stars with colours different from those of the cluster sequences (e.g. Bonatto & Bica 2007a, and references therein). However, residual field stars with colours similar to those of the cluster are expected to remain inside the CM filter. They affect the intrinsic stellar radial distribution profile in a degree that depends on the relative densities of the field and cluster. The contribution of these residual field stars to the RDPs is statistically quantified by means of comparison to the field. In practical terms, the use of the CM filters in cluster sequences enhances the contrast of the RDP with respect to the stellar field. The CM filters are shown in Figs 4–8 as the shaded areas superimposed on the field-star-decontaminated CMDs.

To minimize oversampling near the centre and undersampling for large radii, the RDPs are built by counting stars in concentric rings of increasing width with the distance from the centre. The selected number and width of rings produce RDPs with adequate spatial resolution and moderate 1σ Poisson errors. The residual background level of each RDP corresponds to the average number of CM-filtered stars measured in the comparison field.

The cluster structure was derived by means of a King-like profile, which is similar to a two-parameter King (1962) model that describes the intermediate and central regions of globular clusters. The fit was performed with a non-linear least-squares routine that uses the errors as weights. The best-fitting solutions are shown in Fig. 12 for three relatively populous ECs as a solid line superimposed on the RDPs. The profile is expressed as $\sigma(R) = \sigma_{\rm bg} + \sigma_{0\rm K}/[1 + (R/R_{\rm c})^2]$, where $\sigma_{\rm bg}$ is the stellar background surface density, $\sigma_{0\rm K}$ is the central density relative to the background level and $R_{\rm c}$ is the core radius. The cluster radius ($R_{\rm RDP}$) and uncertainty can be estimated by considering the RDP fluctuations with respect to the residual field. $R_{\rm RDP}$ is the distance from the cluster centre where the RDP and comparison field become statistically indistinguishable. Small variations in the RDPs are probably due to the presence of

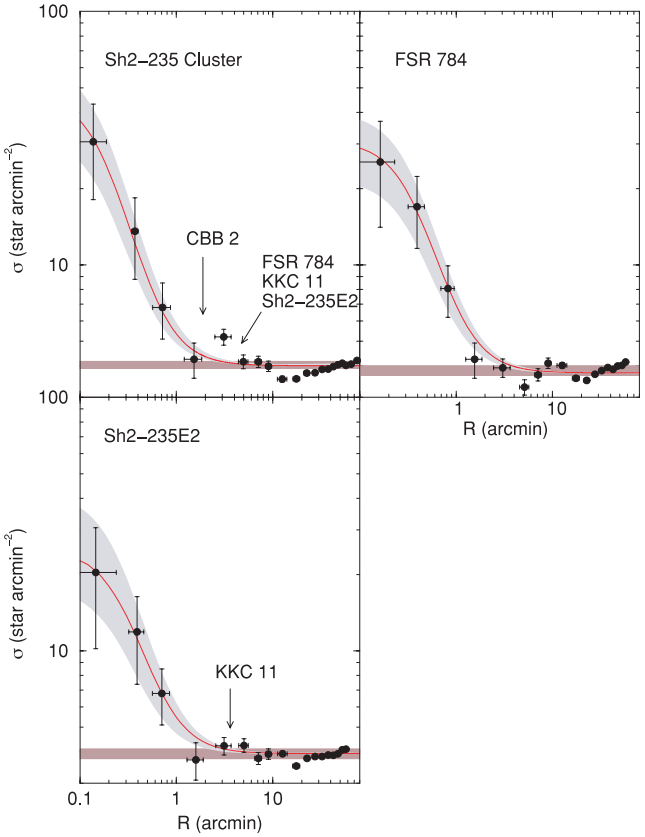

Figure 12. Stellar RDPs (filled circles) built with CM-filtered photometry, centred in the coordinates of Sh2-235 Cluster, FSR 784 and Sh2-235 East2. Solid line: best-fitting King profile. Horizontal shaded region: stellar background level measured in the comparison field. Grey regions: 1σ King-profile-fitting uncertainty.

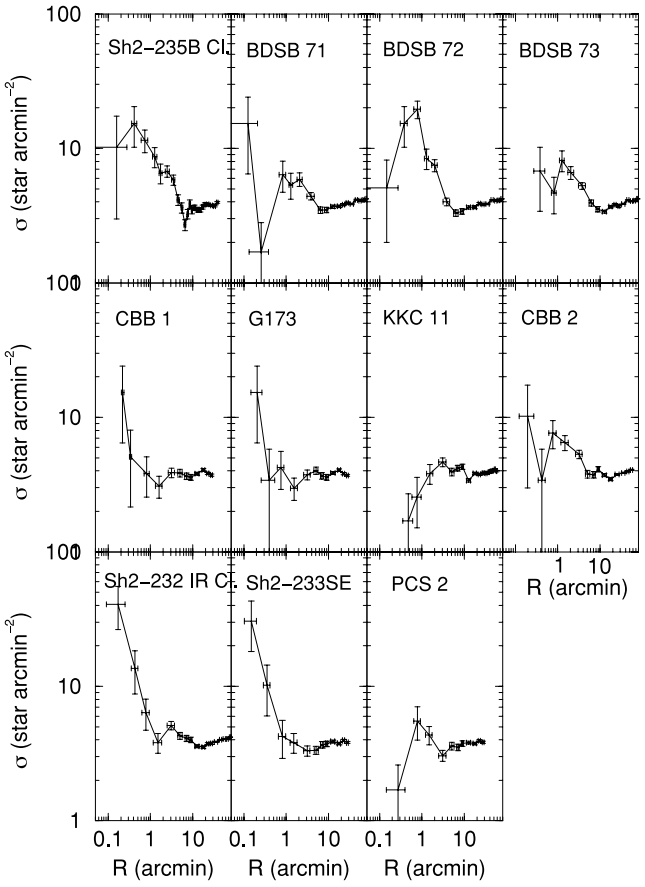

Figure 13. Stellar RDPs for the remaining ECs built with CM-filtered photometry.

other clusters and/or enhanced dust absorption. The derived structural parameters are given in Table 3.

In Fig. 12, we show the RDPs of Sh2-235 Cluster, Sh2-235 East2 and FSR 784. For Sh2-235 Cluster and Sh2-235 East2, overdensities show up in their RDPs.

Fig. 13 shows the RDPs of Sh2-235B Cluster, BDSB 71, BDSB 72, BDSB 73, Sh2-232 IR Cluster, KKC11, CBB 2, and the pairs CBB 1 and G173, and PCS 2 and Sh2-233 SE Cluster. The RDPs are typical of ECs of low-mass and/or initial evolutionary phases, and cannot be fitted by King's profile (Soares et al. 2005). They present bumps and dips as compared to field stars. The depression in star counts in the central region of some ECs is possibly due to strong dust absorption, crowding or structured cores. Sh2-232 IR Cluster has a high cluster/background density contrast, but the profile is irregular. The Sh2-235B Cluster profile includes several of the small clusters nearby like BDSB 71, 72 and 73. A deeper photometry is required for the analysis of the structure of these objects.

The structure of young populous ECs can be generally characterized by an RDP with multiple peaks on a large spatial scale or centrally condensed with an RDP that can be described by a King's law (Lada & Lada 2003), although the present objects are not virialized. However, the differential dust absorption produces conspicuous variations in the RDPs of the present objects. A King profile describes the structure of clusters close to spherical symmetry and centrally concentrated. However, many young clusters are substructured or asymmetric, deviating significantly from this shape, and therefore cannot be fitted by King's law (Cartwright & Whitworth 2004; Gutermuth et al. 2005). In Fig. 14, we show the spatial distribution of stars in the decontaminated photometry of the three ECs that follow a King-like profile (FSR 784, Sh2-235 Cluster

Table 3. Structural parameters.

Cluster	(1 arcmin) (pc)	σ_{0K} (stars pc^{-2})	R_c (pc)	R_{RDP} (pc)	σ_{0K} (stars arcmin^{-2})	R_c (arcmin)	R_{RDP} (arcmin)	ΔR (arcmin)
(1)	(2)	(3)	(4)	(5)	(6)	(7)	(8)	(9)
FSR 784	0.69	56.7 ± 4.0	0.25 ± 0.01	2.1 ± 0.7	27.02 ± 1.9	0.36 ± 0.02	3.0 ± 1.0	$20 - 60$
Sh2-235 East2	0.60	71.7 ± 25.0	0.13 ± 0.03	1.2 ± 0.3	25.8 ± 9.0	0.21 ± 0.05	2.0 ± 0.5	$20 - 80$
Sh2-235 Cluster	0.56	138.1 ± 27.4	0.10 ± 0.01	1.4 ± 0.3	43.32 ± 8.6	0.18 ± 0.02	2.5 ± 0.5	$20 - 80$

Notes. Column (2): arcmin to parsec scale. To minimize degrees of freedom in RDP fits with the King-like profile (see text), σ_{bg} was kept fixed (measured in the respective comparison fields), while σ_0 and R_c were allowed to vary. Column (9): comparison field ring.

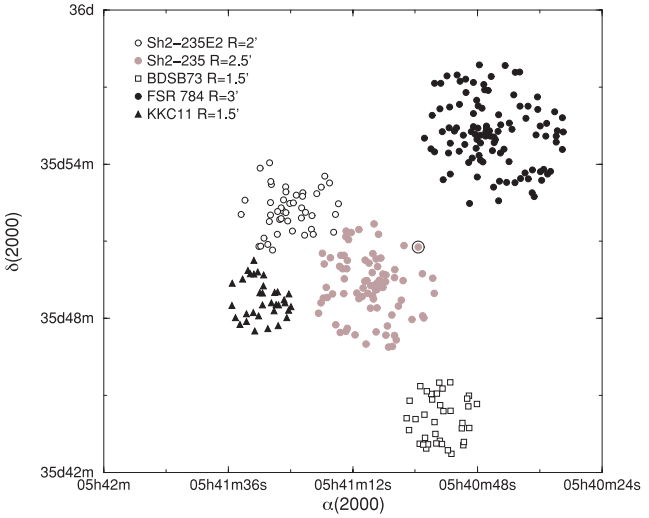

Figure 14. Angular distribution of the decontaminated stellar content for FSR 784, Sh2-235 Cluster, Sh2-235 East2, KKC 11 and BDSB 73. BD +35°1201 is indicated as an open circle around the star.

and Sh2-235 East2) and two representative cases of objects that do not (KKC 11 and BDSB 73). The former are centrally concentrated and nearly circularly symmetric. The cavities and overdensities in the stellar distribution (Fig. 14) can be seen as bumps and dips in the RDP (Fig. 11). On the other hand, objects like BDSB 73 that are not centrally condensed and KKC 11 with more elongated shape do not follow a King profile. The multiple peaks in the RDPs of these ECs may be a fractal effect. If these objects survive the primordial gas expulsion, they may undergo merging evolving into a relatively smooth structure.

The angular distribution of decontaminated stars (Fig. 14), used in the CMD construction, reproduces the distribution of stars in the RDPs built with filtered photometry (Figs 12 and 13), supporting the consistency of our results.

5 MASS ESTIMATES

Given the poorly populated nature of the MS, we simply counted stars in the CMDs (within the region $R < R_{\rm RDP}$) and summed their masses as estimated from the mass–luminosity relation implied by the respective isochrone solutions (Section 3.2). The results are given in Table 4.

All the ECs clearly present distinct populations of MS and PMS stars (Figs 4–8). However, given the differential reddening, it is not possible to attribute a precise mass value for each PMS star. Thus, we simply count the number of PMS stars and adopt an average mass value for the PMS stars to estimate $n_{\rm PMS}$ and $m_{\rm PMS}$. Assuming that the mass distribution of the PMS stars also follows Kroupa's (2001) initial mass function, the average PMS mass – for masses within the range $0.08 \lesssim m(\mathrm{M}_\odot) \lesssim 7$ – is $\langle m_{\rm PMS}\rangle \approx 0.6\,\mathrm{M}_\odot$. Thus, we simply multiply the number of PMS stars (Table 4) by this value to estimate the PMS mass. Finally, we add the latter value to the MS mass to obtain an estimate of the total stellar mass. These values should be taken as lower limits.

6 RELATIONS BETWEEN ASTROPHYSICAL PARAMETERS

N-body simulations of massive star clusters that include the effect of gas removal (e.g. Goodwin & Bastian 2006) show that the phase of dramatic core radii increase may last about 10–30 Myr. Mass segregation may also lead to a phase of core contraction, with high-mass stars more concentrated in the core, while low-mass stars are transferred to outer parts of the cluster. In this context, we suggest that most objects of our sample have not yet removed completely their primordial gas and are not in this expansion phase. As a consequence, the core and cluster radii remain small. However, these ECs may be intrinsically small as well.

Lada & Lada (2003) argue that the structure in ECs reflects the underlying structure in the dense molecular gas from which they formed and suggest two possible structures for these objects: those similar to classical OCs (radially concentrated that fit King's law) and those that exhibit a density profile with multiple peaks. The latter kind of ECs present a fractal-like structure with smaller substructures or mini clusters that are probably a consequence of the fact that these objects are formed in a GMC with a fractal substructure (Schmeja, Kumar & Ferreira 2008; Lomax, Whitworth & Cartwright 2010; Sánchez et al 2010, and references therein). They evolve with time and their fates depend on the processes of dissolution, which they will undergo. If the ECs do not endure the action of the dissolution processes, they might evolve into a homogeneous distribution of stars and eventually disperse. Otherwise, their fate will be a centrally concentrated distribution of stars or a bound cluster. This is possible for the lower mass ECs and cluster pairs or multiples (Figs 4–8). It would also be important to have deeper observations of the less-populated clusters with irregular RDPs (Fig. 13). Probing fainter PMS stars might contribute to the construction of better sampled stellar density profiles, like those of the intrinsically populous and massive clusters in the present star-forming complex (Fig. 12).

When the projected mass density of a star cluster follows a King-like profile (Bonatto & Bica 2008a), the cluster mass ($M_{\rm clus}$) can be expressed as a function of the core radius and the central surface mass density ($\sigma_{\rm M0}$) according to $M_{\rm clus} \approx 13.8\sigma_{\rm M0}R_{\rm c}^2$ (Bonatto & Bica 2009). Fig. 15 (top right-hand panel) shows the distribution of our populous ECs in the plane core radius (Section 4) versus cluster

Table 4. Stellar mass estimate for more populous ECs.

		MS		PMS		MS+PMS	
Cluster	$\Delta\, m_{\rm MS}$ ($\mathrm{M}_\odot$)	N (stars)	M ($\mathrm{M}_\odot$)	N (stars)	M ($\mathrm{M}_\odot$)	N (stars)	M ($\mathrm{M}_\odot$)
(1)	(2)	(3)	(4)	(5)	(6)	(7)	(8)
FSR 784	2.90–4.30	3 ± 1	9 ± 4	65 ± 15	39 ± 9	68 ± 16	48 ± 13
Sh2-235 East2	2.50–5.25	6 ± 2	24 ± 9	41 ± 6	25 ± 4	47 ± 8	49 ± 13
Sh2-235 Cluster	1.30–6.25	5 ± 2	22 ± 7	67 ± 15	40 ± 9	72 ± 17	62 ± 16

Notes. Column (2): MS mass range. Columns (3)–(6): stellar content of the MS and PMS stars. Columns (7) and (8): total (MS+PMS) stellar content.

Table 5. Integrated colours and magnitudes.

	Magnitude						Colour	
Cluster	Apparent			Absolute			Reddening	Corrected
	J	H	K_S	J	H	K_S	$(J-H)$	$(J-K_S)$
(1)	(2)	(3)	(4)	(5)	(6)	(7)	(8)	(9)
FSR 784	12.9	9.7	8.8	−0.02	−2.8	−4.0	2.82 ± 0.14	3.57 ± 0.14
Sh2-235 East2	13.2	11.7	10.6	0.5	−0.6	−1.5	1.11 ± 0.33	1.99 ± 0.31
Sh2-235 Cluster	8.5	8.2	7.9	−4.0	−4.0	−4.0	-0.05 ± 0.04	0.01 ± 0.04

Notes. Columns (2)–(4): apparent magnitude. Columns (5)–(7): absolute magnitude. Columns (8) and (9): $(J-H)$ and $(J-K_S)$ colours.

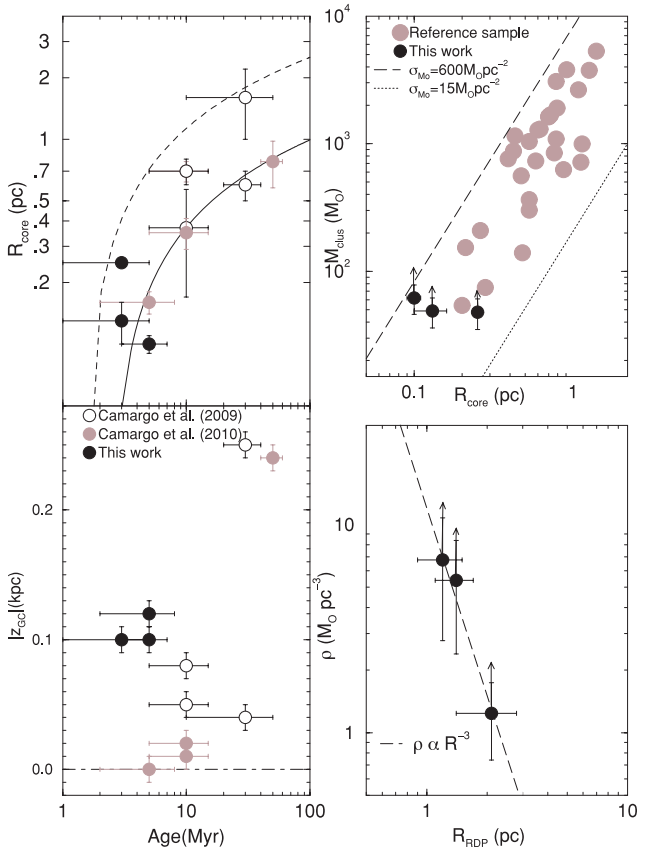

Figure 15. Present cluster properties compared with literature ones (Camargo et al. 2009; 2010). Top left-hand panel: age and R_c relations. The dashed line is the logarithmic fit of Bastian et al. (2008) $\{R_c(\mathrm{pc}) = 0.6 \times \ln[\mathrm{age\,(Myr)}] - 0.25\}$ for M51 clusters. The solid line is our fit for Galactic clusters. Bottom left-hand panel: $|z_{GC}|$ for clusters of the top left-hand panel. Top right-hand panel: core radius and cluster mass follow the relation $M_{clus} = 13.8\sigma_{M0}R_c^2$, with varying values of σ_{M0}; reference sample OCs are shown as the grey circles. Bottom right-hand panel: cluster density versus radius. The arrows indicate lower limits to the cluster mass and density.

mass (Section 5). Clearly, our ECs (together with the reference sample) distribute parallel to the above relation, being constrained within King-like distributions with $15 \lesssim \sigma_{M0}\,(\mathrm{M_\odot\,pc^{-2}}) \lesssim 600$ (these limits take the uncertainties into account). This correlation between the cluster mass and core radius is consistent with the mass–radius relation suggested by Portegies Zwart, McMillan & Gieles (2010) for massive clusters younger than 100 Myr and extended for less-massive ones (Camargo, Bonatto & Bica 2010).

Since the cluster radius and mass were estimated, we compute the cluster mass density $\rho(\mathrm{M_\odot\,pc^{-3}}) = \frac{3}{4\pi} M_{clus}\, R_{RDP}^{-3}$. The results are shown in the R_{RDP} versus ρ plane (Fig. 15, bottom right-hand panel). Despite the error bars, the density decreases with the cluster radius as $\rho \propto R_{RDP}^{-(3.0\pm0.3)}$, similarly to the cluster sample studied by Camargo et al. (2010). We also show in Fig. 15 the relation between age and both R_c and $|Z_{GC}|$ for the present ECs. We fit an empirical curve $R_c(\mathrm{pc}) = 0.27 \times \ln[\mathrm{age\,(Myr)}] - 0.25$ (solid line) to Galactic OCs younger than 100 Myr. The dashed line is the observed relation for M51 clusters (Bastian et al. 2008). The present clusters behave as relatively low mass ECs, as expected.

Finally, in Table 5 we show integrated colours and magnitudes for those clusters that follow a King-like profile.

7 CONCLUDING REMARKS

In this work, we performed a field-star-decontaminated 2MASS analysis of 14 ECs in the H II regions Sh2-235, Sh2-233, Sh2-232 and Sh2-231, and other small nebulae in the area. We were able to derive astrophysical parameters and investigate the nature of young clusters embedded in these H II regions. Fundamental parameters were obtained for all ECs analysed, but structural parameters were derived for FSR 784, Sh2-235 East2 and Sh2-235 Cluster. The decontaminated CMDs exhibit a poorly populated MS and a large fraction of PMS stars, and suggest some age spread, as expected for a sequential star formation process. Two new ECs (CBB 1 and CBB 2) were discovered in this work.

The age, size and location of KKC 11, FSR 784, Sh2-235 Cluster, CBB 2 and Sh2-235 East2 are consistent with the *collect-and-collapse* scenario. The CMDs of Sh2-235B Cluster, BDSB 71, BDSB 72, BDSB 73, Sh2-232 IR Cluster, G173, CBB 1 and PCS 2 suggest that these objects are ECs. The enhanced dust absorption, mainly in the innermost region, indicates that deep photometry is necessary to derive their structural parameters.

The present ECs have core and cluster radii smaller than those of clusters at the same Galactocentric distance and age. Probably, most of them have not expelled the primordial gas completely and thus have not expanded.

ACKNOWLEDGMENTS

We thank an anonymous referee for important comments and suggestions. This publication makes use of data products from the Two-Micron All-Sky Survey, which is a joint project of the University of Massachusetts and the Infrared Processing and Analysis Centre/California Institute of Technology, funded by the National Aeronautics and Space Administration and the National Science Foundation. This research has made use of the WEBDA data

base, operated at the Institute for Astronomy of the University of Vienna, as well as Digitised Sky Survey images from the Space Telescope Science Institute obtained using the extraction tool from the CADC (Canada). We acknowledge support from CNPq and CAPES (Brazil).

REFERENCES

Allen L. E., Hora J. L., Mergeath S. T., Deutsch L. K., Fazio G. G., Chavarria L., Dell R. D., 2005, in Cesaroni R., Churchwell E., Felli M., Walmsley C. M., eds, Massive Star Birth: A Crossroads of Astrophysics. Cambridge Univ. Press, Cambridge, p. 352
Allen L. E., Mergeath S. T., Gutermuth R., Myers P. C., Wolk S., Adams F. C., Muzerolle J., Pipher J. L., 2007, in Reipurth B., Jewitt D., Keil K., eds, Protostars and Planets V. Univ. Arizona Press, Tucson, p. 361
Bastian N., Gieles M., Goodwin S. P., Trancho G., Smith L. J., Konstantopoulos I., Efremov Yu., 2008, MNRAS, 389, 223
Bica E., Dutra C. M., Soares J., Barbuy B., 2003, A&A, 404, 223
Bica E., Bonatto C., Barbuy B., Ortolani S., 2006, A&A, 450, 105
Bica E., Bonatto C., Camargo D., 2008, MNRAS, 385, 349
Blitz L., Fich M., Stark A. A., 1982, ApJS, 49, 183
Boley P. A., Sobolev A. M. et al., 2009, MNRAS, 399, 778
Bonatto C., Bica E., 2007a, A&A, 473, 445
Bonatto C., Bica E., 2008a, A&A, 477, 829
Bonatto C., Bica E., 2009, MNRAS, 397, 1915
Bonatto C., Bica E., 2011, preprint (arXiv:1103.2293)
Bonatto C., Bica E., Girardi L., 2004, A&A, 415, 571
Bonnell I. A., Dobbs C. L., Robitaille T. P., Pringle J. E., 2006, MNRAS, 365, 37
Camargo D., Bonatto C., Bica E., 2009, A&A, 508, 211
Camargo D., Bonatto C., Bica E., 2010, A&A, 521, 42
Cardelli J. A., Clayton G. C., Mathis J. S., 1989, ApJ., 345, 245
Carpenter J. M., Snell R. L., Schloerb F. P., Shrutskie M. F., 1993, ApJ, 407, 657
Cartwright A., Whitworth A. P., 2004, MNRAS, 348, 589
Chan G., Fich M., 1995, AJ, 109, 2611
Dale J. E., Bonnell I. A., Whitworth A. P., 2007, MNRAS, 375, 1291
Deharveng L., Zavagno A., Salas L., Porras A., Caplan J., Cruz-González I., 2003, A&A, 399, 1135
Deharveng L., Zavagno A., Caplan J., 2005, A&A, 433, 565
Dewangan L. K., Anandarao B. G., 2011, MNRAS, 414, 1526
Dobashi K., Yonekura Y., Matsumoto T., Momose M., Sato F., Bernard J.-P., Ogawa H., 2001, PASJ, 53, 85
Dutra C. M., Bica E., 2001, A&A, 376, 434
Dutra C. M., Santiago B. X., Bica E., 2002, A&A, 383, 219
Elmegreen B. G., 2000, ApJ, 530, 277
Elmegreen B. G., Lada C. J., 1977, ApJ, 214, 725
Felli M., Testi L., Valdettaro R., Wang J.-J., 1997, A&A, 320, 594
Felli M., Massi F., Navarrini A., Neri R., Cesaroni R., Jenness T., 2004, A&A, 420, 553
Froebrich D., Scholz A., Raftery C. L., 2007, MNRAS, 374, 399
Fukuda N., Hanawa T., 2000, ApJ, 533, 911
Georgelin Y. M., 1975, PhD Thesis, Universitè de Provence, Observatoire de Marseille
Georgelin Y. M., Georgelin Y. P., Roux S., 1973, A&A, 25, 337
Girardi L., Bertelli G., Bressan A., Chiosi C., Groenewegen M.-A.-T., Marigo P., Salasnich B., Weiss A., 2002, A&A, 391, 195
Goodwin S. P., Bastian N., 2006, MNRAS, 373, 752
Gouliermis D. A., Chu Y. H., Henning T., Brandner W., Gruendl R. A., Hennekemper E., Hormuth F., 2008, ApJ, 688, 1050
Gutermuth R. A., Megeath S. T., Pipher J. L., Williams J. P., Allen L. E., Myers P. C., Raines S. N., 2005, ApJ, 632, 397
Hartmann L., Ballesteros-Paredes J., Bergin E. A., 2001, ApJ, 562, 852
Hodapp K.-W., 1994, ApJS, 94, 615
Hosokawa T., Inutsuka S., 2005, ApJ, 623, 917
Jiang Z., Yao Y., Yang J., Ishii M., Nagata T., Nakaya H., Sato S., 2001, AJ, 122, 313
King I., 1962, AJ, 67, 471
Kirsanova M. S., Sobolev A. M., Thomasson M., Wiebe D. S., Johansson L.-E.-B., Sekznev A.-F., 2008, MNRAS, 388, 729
Koposov S. E., Glushkova E. V., Zolotukhin I. Yu., 2007, A&A, 486, 771
Kumar M. S. N., Keto E., Clerkin E., 2006, A&A, 449, 1033
Lada C. J., Adams F. C., 1992, ApJ, 393, L278
Lada C. J., Lada E. A., 2003, ARA&A, 41, 57
Lada C. J., Margulis M., Dearborn D., 1984, ApJ., 285, 141
Lafon G., Deharveng L., Baudry A., de La Noe J., 1983, A&A, 124, 1
Lefloch B., Lazareff B., 1994, A&A, 289, 559
Leisawitz D., Bash F. N., Thaddeus P., 1989, ApJS, 70, 731
Lomax O., Whitworth A. P., Cartwright A. T., 2010, preprint (arXiv:1010.5944)
Mao R.-Q., Zeng Q., 2004, Chin. J. Astrophys., 5, 440
Porras A., Cruz-Gonzàles I., Salas L., 2000, A&A, 361, 660
Portegies Zwart S. F., McMillan S., Gieles M., 2010, ARA&A, 48, 431
Proszkow E. M., Adams F. C., 2009, ApJS, 185, 486
Sánchez N., Anez N., Alfaro E. J., Odekon M. C., 2010, ApJ, 720, 541
Saurin T. A., Bica E., Bonatto C., 2010, MNRAS, 407, 133
Schmeja S., Kumar M. S. N., Ferreira B., 2008, MNRAS, 389, 1209
Shepherd D. S., Churchwell E., 1996, ApJ, 472, 225
Shepherd D. S., Watson A. M., 2002, ApJ, 566, 966
Siess L., Dufour E., Forestini M., 2000, A&A, 353, 593
Skrutskie M. F. et al., 2006, AJ, 131, 1163
Snell R. L., Dickman R. L., Huang Y. -L., 1990, ApJ, 352, 139
Soares J. B., Bica E., Ahumada A. V., Clarià J. J., 2005, A&A, 430, 987
Tokunaga A. T., Thompson R. I., 1979, ApJ, 233, 127
Varricatt W. P., Davis C. J., Adamson A. J., 2005, MNRAS, 359, 2
Verschueren W., 1990, A&A, 234, 156
Wang J. -J., Testi L., Felli M., 1997, in Malbet F., Castets A., eds, Proc. IAU Symp. 182, Low Mass Star Formation - from Infall to Outflow. Kluwer, Dordrecht, p. 48
Whitworth A. P., Bhattal A. S., Chapman S. J., Disney M. J., Turner J. A., 1994, MNRAS, 268, 291
Wouterloot J. G. A., Brand J., 1989, A&AS, 80, 149
Yan C.-H., Minh Y. C., Wang S.-Y., Su Y.-N., Ginsburg A., 2010, ApJ, 720, 1

This paper has been typeset from a TEX/LATEX file prepared by the author.